03

Experimental investigation of nanofluid boiling in thermosyphons

© V.M. Kiseev, O.V. Sazhin

Institute of Natural Sciences and Mathematics, Ural Federal University,
620002 Yekaterinburg, Russia
e-mail: oleg.sazhin@urfu.ru

Received May 22, 2023
Revised July 8, 2023
Accepted July 24, 2023

Studies of the heat transfer coefficient and thermal resistance for a loop thermosyphon with a high heat flux density in the transport zone, as well as studies of the critical heat flux using a traditional thermosyphon, have been carried out. Measurements were carried out for pure water, water with porous coatings of the vaporization surface and nanofluid, all other things being equal, using technically polished copper surfaces as the boiling surface. The mechanism of formation of nanorelief on the vapor-generating surfaces of thermosyphons and an increase in the heat transfer coefficient and critical heat flux due to this is revealed. A dynamic model of the formation of this nanorelief is proposed. Accelerated and long-term life-test of a loop thermosyphon filled with water with iron oxide and copper oxide nanoparticles were carried out, and its stable performance was shown.

Keywords: two-phase heat transfer devices, heat transfer coefficient, critical heat flux, nanofluid, thermosyphon, heat carrier, thermal resistance.

DOI: 10.61011/TP.2023.10.57446.134-23

Introduction

The problem of efficient transfer of heat energy and thermal control of various systems and equipment is one of the key problems of modern thermal physics. A phase transition and heat and mass transfer associated with this process and occupying a special place among the physical phenomena used in nature and technology are often used to solve this problem. In this regard, studies of potential nanofluidic heat carriers have become of increased interest and widespread.

The concept of nanofluids first proposed by S.U. Choi and J.A. Eastman [1], which is actually a suspension of nanoparticles, has been studied by many researchers. Currently, the focus is on phase-varying heat transfer of nanofluids, while previously they were analyzed for thermal conductivity and heat transfer in a single-phase flow [1–6]. The use of nanofluids for phase-varying heat transfer in heat pipes [7–14] is becoming increasingly popular.

Many experiments have been conducted on the germinal boiling of nanofluids over the past decade both in large volume and in real heat transfer devices (heat pipes and thermosyphons). The number of publications in this field, often contradictory, number in the hundreds [15–19]. We have taken as a basis the review papers [20,21]. The review by Jadhava and colleagues [20] is of particular interest, it analyzes the available studies and presents the key problems preventing the strengthening of critical heat flux (CHF). The following statements can be quoted among the conclusions of this review.

1. CHF of nanofluid depends on type of material of nanoparicles. In nanofluid pool boiling nanoparticles deposits on heater surface and form coating. Those nanopaticle material having shorter Rayleigh.Taylor wavelengths when coated on heater surface shows higher CHF enhancement while material having larger Rayleigh.Taylor wavelengths shows lower CHF enhancement.

2. For nano particles size within nano range there is no significant variation in CHF. But comparing particle size within nano and micro range there is significant enhancement in CHF for particle size in nano range than particle size in micro range.

3. With increasing nanoprticle concentrations CHF enhancement occurs up to certain concentration then CHF enhancement decreases with increase in nanoparticle concentration. Researchers mentioned nanoparticle depositions on heater surface are responsible for CHF enhancement. Detail effect of nanoparticles concentrations on surface modifications needs to be find out which leads to CHF enhancement.

H. Ghorabaee and colleagues presented a comprehensive review of studies of the dominant heat transfer mechanisms when using nanofluids in traditional thermosyphons (TTS) [21]. In particular, the impact of the supplied heat, the type and concentration of nanoparticles on the thermal characteristics of the TTS was generalized. As a result, the authors came to a number of conclusions, namely, nanofluids significantly improve the thermal characteristics of TTS by reducing thermal resistance and increasing the thermal efficiency of TTS; thermal characteristics of TTS strongly depend on the operating parameters, especially on the type of nanoparticles, their concentration and addition of surfactant, as well as on heat loads; in addition, thermalt characteristics of TTS with different heat input surprisingly depend on the type of nanofluid. This review also shows a wide range of applications of nanofluid-based heat pipes in

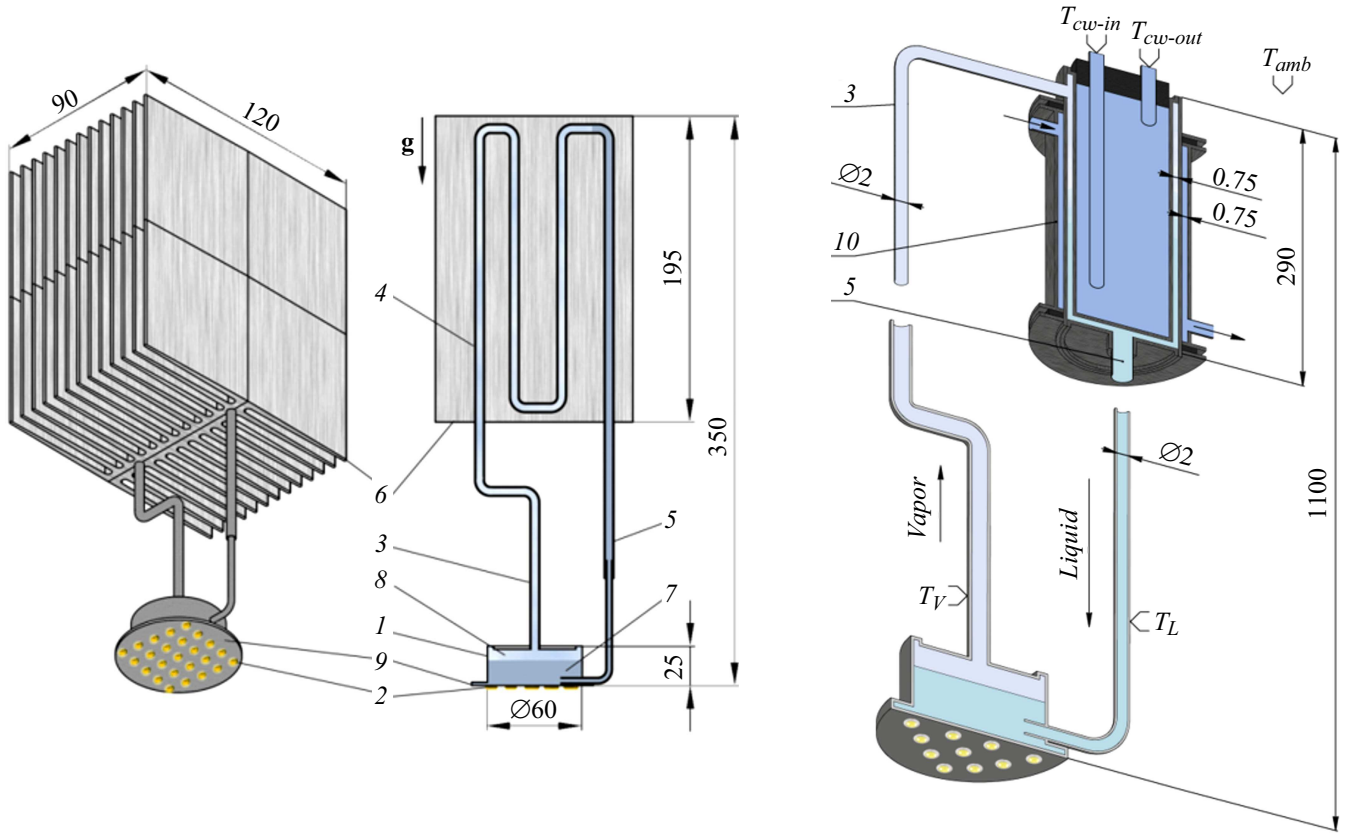

Figure 1. Schematic diagram of loop thermosyphons LTS1 (left) and LTS2 (right) used for cooling the LED matrix: *1* — evaporator; *2* — LEDs; *3* —steam channel; *4* — condenser; *5* — liquid channel; *6* —radiator; *7* — liquid; *8* — steam; *9* —LED matrix; *10* — water-cooled shell. The figure shows the direction of gravity.

energy systems. In conclusion, some problems are identified and suggestions are made to improve future research.

Thus, analyzing the results of experimental studies of phase transformations in the nonequilibrium system „nanofluid–steam“, presented in the open literature, it is possible to conclude that the mechanisms of heat transfer on the surface of vaporization have not been studied in detail and the possibilities of long-term use of thermosyphon systems are not discussed, and obtaining a stable nanofluid is still quite a difficult task. In addition, there are many contradictions in terms of explaining the effect of nanofluids on improving heat transfer in two-phase heat exchange devices, and most studies do not consider long-term tests. It is for this reason that this study covers traditional thermosyphon systems and focuses on determining the effect of nanofluid on heat exchange in a loop thermosyphon filled with iron oxide/water and copper oxide/water nanofluids. The main objectives of our studies are:

- to use nanofluids as heat carriers (including long-life testing) for temperature control devices, and compare the results obtained with the results for clean working fluids;
- to obtain the distribution of nanoparticles before and after use in a loop thermosyphon;
- to develop a thermal control system based on loop thermosyphons for LED modules (and other similar sources of heat generation) with a flat cylindrical evaporator and a frontal heat load;
- to investigate the boiling crisis of nanofluid in a traditional thermosyphon, and compare these data for pure water and on porous coatings of the vaporization surface.

1. Experimental devices and techniques

1.1. Experimental setup for loop thermosyphon research

The loop thermosyphon (LTS) is shown in Fig. 1. It includes the following components: the evaporator cavity *1* for steam *8* and liquid *7*, the steam channel *3* and the liquid channel *5*, interconnected by the evaporator *1* and the coil (LTS1) condensator *4* located in the radiator *6*. Steam channel *3*, liquid channel *5* and condenser *4* LTS can be made of flexible tubes, while the radiator *6*, in which the capacitor is placed *4*, can be located anywhere (above the evaporator) with maximum natural convection. The liquid channel *5* collects a column of liquid with this arrangement of the radiator with a pressure drop ΔP_g after steam condensation in the condenser *4*. This ensures the return of condensate to the evaporator *1*, thereby completing the „evaporation-condensation“ cycle and ensuring the

circulation of the working fluid. LEDs *2* are located on a heat-conducting metal substrate (LED matrix) *9*, namely on the lower surface of the evaporative cavity *1*. The LTS, from which the air was previously removed (pumping to a pressure of 10^{-2} mbar), is filled with working fluid. LEDs when activated *2* emit light energy and emit thermal energy, which is transmitted through the substrate *9* of the liquid *7* in the cavity of the evaporator *1*. The liquid evaporates or boils (depending on the heat flux) and turns into steam. The steam *8* has a higher pressure than the steam in the condenser *4*, due to the temperature difference between them.

Thus, the steam passes through the steam channel *3* into the condenser *4*, where it releases its latent heat when converted to liquid (condensation). The heat released in the condenser is then radiated into the environment by the radiator *6*. Under the impact of gravity, the formed condensate returns through the liquid channel *5* to the evaporator cavity *1*, thereby closing the evaporation-condensation heat exchange cycle. The diameter of the liquid channel was reduced and immersed in the liquid of the evaporator to prevent the movement of steam through the liquid channel, i.e. to ensure its movement through the steam channel when starting the LTS *7*. The LTS evaporator was a copper cavity in the form of a tablet with an outer diameter of 60 mm, a height of 25 mm and a wall thickness of 2 mm. The steam channel, the coil condenser (four sections of vertical pipes: three turns in increments of 25 mm), the liquid channel and the inlet liquid channel were made of copper tubes with an inner diameter of 4×1 mm, 4×1 mm, 2×0.5 mm and 1×0.25 mm respectively. $120 \times 195 \times 90$ mm ribbed radiator (LTS1) was used to transfer the released heat to the environment. The total area of the ribbed surface of the radiator (LTS1) was 0.48 m^2. A coil condenser was installed on the inner surface of the radiator. Two halves of the radiator were bolted together using a thermal paste so that the coil was inside the radiator. The radiator was made of aluminum. The dimensions of the LTS are shown in Fig. 1. LTS2 differed from LTS1 by a coaxial (pipe in a pipe with an internal diameter of 23 mm, length 290 mm, with an internal gap of 0.75 mm) water-cooled condenser to provide a greater heat load, and had a total height of 1100 mm. The steam and liquid channels had smaller internal diameters —2×0.5 mm to realize heat transport similar to electricity transport.

Both an LED matrix and a MINCO resistive film heater (LTS1) were used as a heater, while a more powerful resistive heater in the form of a tablet was used for LTS2. The heaters were attached using a heat-conducting paste to the surface of the evaporator, they were carefully insulated and checked for heat dissipation to the outside. The deviation from the nominal heat load did not exceed 3%.

Figure 2 shows the scheme of the experimental setup and the location of thermocouples. The experimental study involves obtaining temperatures at certain points of the loop thermosyphon depending on the nominal thermal load. The

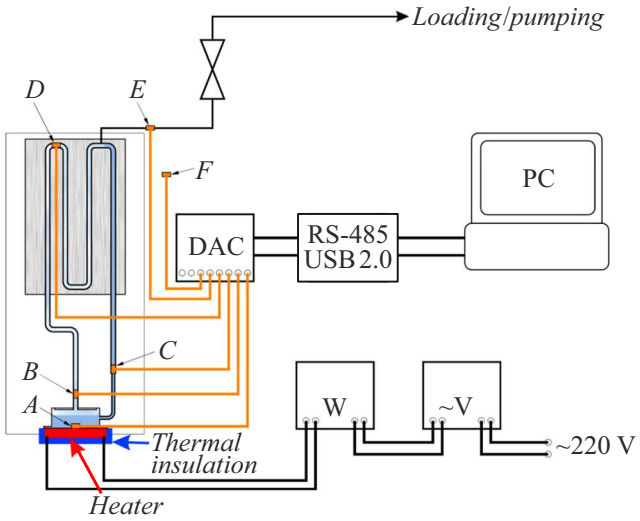

Figure 2. Schematic diagram of an experimental installation for measuring temperature in certain places of the thermosyphon: *A*–*F* — locations of thermocouples; DAS — data acquisition system; W — wattmeter; V — voltmeter.

heat load is designed to simulate the actual heat flux of LEDs. The following locations on the thermosyphon were selected: *A* — between the evaporator and the heater; the temperature was measured T_{ev} on the heater wall; *B* — the upper point of the evaporator; the vapor temperature was measured T_v; *C* — near the evaporator inlet; the temperature of the liquid in the condenser pipe was measured T_l and *F* — ambient temperature measurement T_{amb}.

1.2. Experimental setup for studying the boiling process in traditional thermosyphon

An experimental setup was developed and manufactured to study vaporization during boiling of nanofluids, the schematic drawing of which is shown in Fig. 3.

The experimental installation is a traditional thermosyphon with an end heat supply from a thermal wedge. It allows measuring the heat transfer coefficient in a wide range of changes in the heat flux density and saturation pressure of the working fluid. The heat wedge *1* was a copper part consisting of two cylinders: a cylinder with a diameter of 80 mm and a height of 140 mm, containing an ohmic heater, and a second cylinder with a diameter of 20 mm and a length of 60 mm, which is a working surface for installation. There was a dead-end hole with a diameter of 2 mm to accommodate the thermal sensor (copper-constantan thermocouple located at the point *E*, in Fig. 3), which measures the temperature of the heating surface of the contact with the working fluid ($T_E = T_{ev} = T_h$). There was another hole directed to the center of the cylinder (T_F) at a distance of $l = 30 \pm 0.1$ mm below. The heat flux was measured using these thermocouples and the temperature difference ($T_E - T_F$). The thermal wedge was attached to

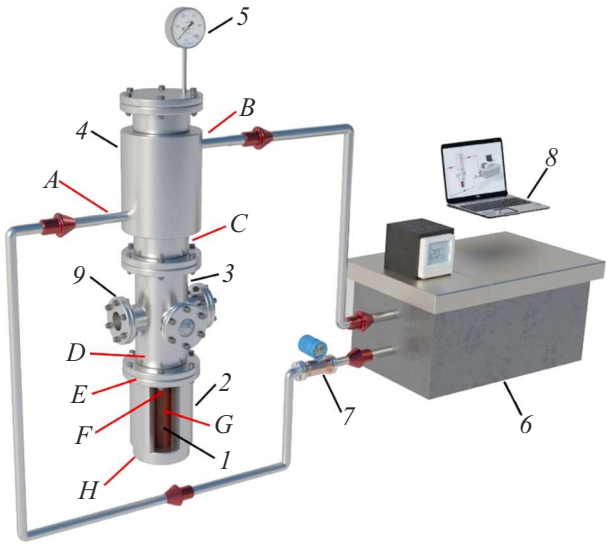

Figure 3. Schematic diagram of an experimental installation for measuring the heat transfer coefficient (HTC) and critical heat flux (CHF): *1* — electric heater with thermal wedge; *2* — protective heater; *3* — working chamber; *4* —condenser; *5* — pressure gauge; **6** — thermostat; *7* — flow meter; *8* — data collection systems, *9* — viewing window. *A*–*H* — location of thermocouples.

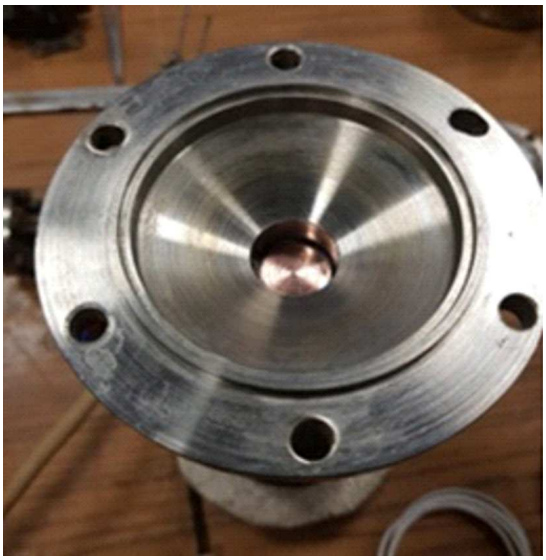

Figure 4. The heating surface of the copper wedge.

the flange of the working chamber with silver solder (Fig. 4). The sealed working chamber *3* for visual observations is provided with viewing windows, one of which is designed for lighting. There is a capacitor *4* in the upper part of the working chamber with a total condensation surface of 300 cm^2. A pressure gauge *5* is installed on the upper flange.

The thermostatically controlled water was circulated using thermostat U-16 to discharge heat from the condenser with a given flow rate *6*. The water flow rate (at water temperature 20–40°C and mass flow through the heat exchanger up to 40 g/s) was measured using a flow meter *7* with an error of 1 g/s.

Copper-constantan thermocouples (type of thermocouple T Z2-T-PFA-TT-1/0.08-1.0-T) located in certain places were used to control the operating temperatures of research facilities (Fig. 2, 3). The temperature was recorded as follows. After the voltage was applied and the input power (heat load) was measured, the data acquisition system began to measure the temperature over time. Then, when the temperature stabilized, the experimental launch continued to 1 h, while the temperature was still recorded by the DAS instrument (Russia, Owen TRM-148) *8*. Finally, after the experiment was completed, the measured temperatures were averaged and the standard deviation was calculated. The maximum error of measuring the temperature of the thermocouple was 0.2 K. The maximum error of the power meter (digital wattmeter CP3010) was 0.1% of the final value of the power measurement range, and the maximum error of the heat transfer coefficient (HTC) and critical heat flux (CHF) was estimated at 3.5%. The surface of the heat wedge was surrounded by a protective heater to prevent heat leakage into the environment *2*.

The heat flow was measured in three ways.

1. Measurement of the electrical power supplied to the main heater.

2. Measurement of heat flow along a thermal wedge due to its thermal conductivity in accordance with Fourier's law:

$$Q = -k\nabla T S_h \approx k(T_E - T_F)S_h/l, \tag{1}$$

where k — the thermal conductivity of the copper wedge and $(T_E - T_F)/l$ — the temperature gradient at the specified points of placement of thermocouples on the thermal wedge, S_h — the cross section of the thermal wedge.

3. The heat flux for a given mass flow rate $\dot{m}$, [kg/s] of the water cooling the condenser, its specific heat capacity c_l, [J/(kg·K)] and the temperature difference at the inlet (T_A) and the outlet (T_B) of the condenser cooling jacket

$$Q = \dot{m}c_l(T_B - T_A). \tag{2}$$

The heat transfer coefficient (HTC) h was determined by the expression

$$h = \frac{Q}{S_h}/(T_E - T_D); \quad S_h = \frac{\pi d^2}{4}, \tag{3}$$

where $q = Q/S_h$ — heat flux density, d — diameter of the second cylinder and $T_v = T_D$ — steam temperature.

1.3. Preparation of nanofluids

According to the methodology proposed by Asadi and colleagues, the preparation of nanofluid was a three-step procedure [6]. First, a highly dispersed powder Fe_xO_y was added to distilled and deionized water in the cylinder (or Cu_xO_y were manufactured and studied at the Institute of

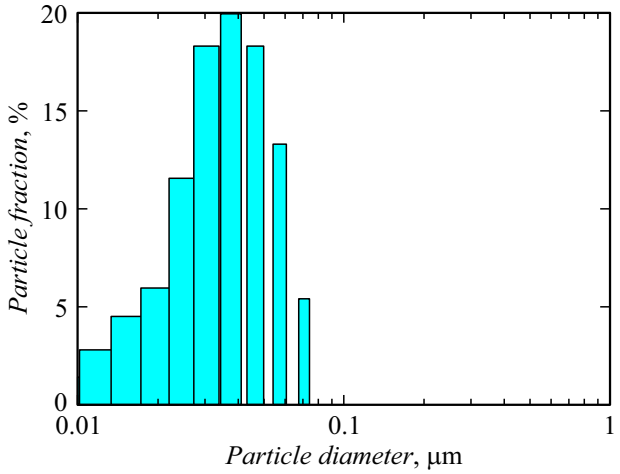

Figure 5. Typical particle size distribution in nanofluid.

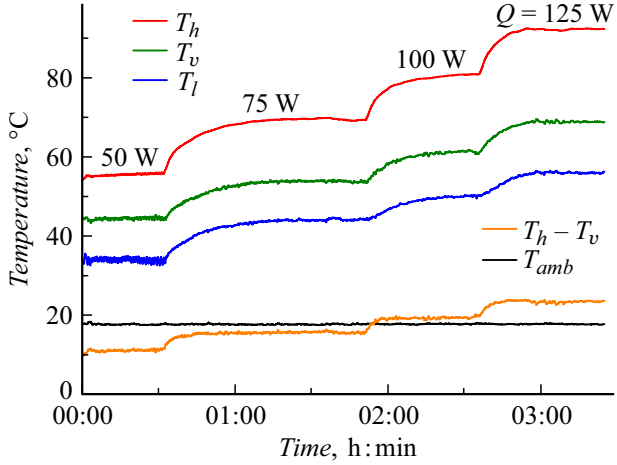

Figure 6. Basic temperatures of LTS1 with nanofluid Fe_xO_y/water (mass concentration: $w = 2.0\%$) at various heat loads Q.

Electrophysics of the Ural Branch of the Russian Academy of Sciences, Yekaterinburg (http://iep.uran.ru). Metal oxides are selected due to their affinity with the materials and heat carriers used in the LTS and weak chemical activity, which is important for closed two-phase systems due to possible gas release and blocking of the condensation zone, leading to deterioration of the thermal characteristics of heat pipes and thermosyphons.

The resulting mixture was placed in an ultrasonic dispersant with a power of up to 5 kW per 10–15 min. Ultrasonic vibration methods are widespread, and most researchers use these methods to obtain stable nanofluids. The mixture was placed in SHIMADZU SALT-7101 laser particle size analyzer, which measured the particle size distribution for assessment of the quality of the prepared nanofluid. Typical measurement results are shown in Fig. 5. This procedure was repeated with each solution. The prepared solutions had the following mass concentrations: $w = 2.0$, 1.5, 1.0 and 0.5%. The particle size distribution was from 15 to 75 nm for Fe_xO_y and from 35 to 105 nm for Cu_xO_y.

2. Findings and discussion

2.1. Two-phase LTS with nanofluids

The experimental technique assumed obtaining data on the operating parameters of the LTS in the form of a relationship between the temperature of the control points and the heat load Q. The impact of the refilling volume is insignificant, however, the minimum temperature corresponded to the refueling volume of 15 ml for LTS1 (25% of the full refueling equal to 61 ml or 31% of the evaporator volume equal to 48 ml), and further measurements were performed with this refilling volume. The thickness of the liquid layer in the evaporator LTS1 (in the absence of heat load) with such refilling (15 ml) is about 6 mm. The LTS temperatures were measured at the points A–F indicated in Fig. 2. Measurements were performed before and after the transition of the system to steady-state mode for each heat load Q. Figure 6 shows the main temperatures of LTS1, namely the temperature in the contact zone of the heater and the evaporator surface T_h, the vapor temperature at the outlet of the evaporator T_v, the liquid temperature at the inlet of the evaporator T_l, the temperature difference $T_h - T_v$ and ambient temperature T_{amb} under various heat loads and natural convection of the radiator in the case of mass concentration of nanoparticles $w = 2.0\%$.

We calculated the heat transfer coefficient (HTC) during evaporation using the equation (3), where Q — heat load; S_h — the surface area of the supplied heat $23.7 \cdot 10^{-4}\,\mathrm{m}^2$ (LTS1 and LTS2); and T_h and T_v — heater and steam temperatures at points A and B (fig. 2) respectively. The maximum heat flow (CHF) was not studied due to the limited surface of the radiator for natural convection.

The experimental results shown in Fig. 7 demonstrate the effect of mass concentrations on the increase of HTC (h) nanofluid (LTS1) ($w = 0$, 1.0, 1.5 and 2 mass%). At a concentration of $w = 2.0\%$, the increase is 20–25%, taking into account that the LTS itself is an effective heat transfer device.

The complexity of germinal vaporization processes is such that accurate, reliable design theories based on analysis are not yet available. As a consequence, completely empirical methods are used to predict the heat transfer coefficients during boiling in a large volume. The wall overheating ΔT depending on the heat flux density q is measured in a large-volume boiling experiment, and the heat transfer coefficient at germinal boiling is obtained from its determination ($h \equiv q/\Delta T$). Literally hundreds of large volume boiling correlations have been proposed. Boiling correlations in this case are usually formulated in such a way that expressions in the form $h \propto q^n$ (n of the order of 2/3 or 0.7) it is easiest to apply, since the heat flow is a given design variable, while the wall temperature at ΔT is unknown and is part of the solution. The classical Labuntsov correlation (1973) is

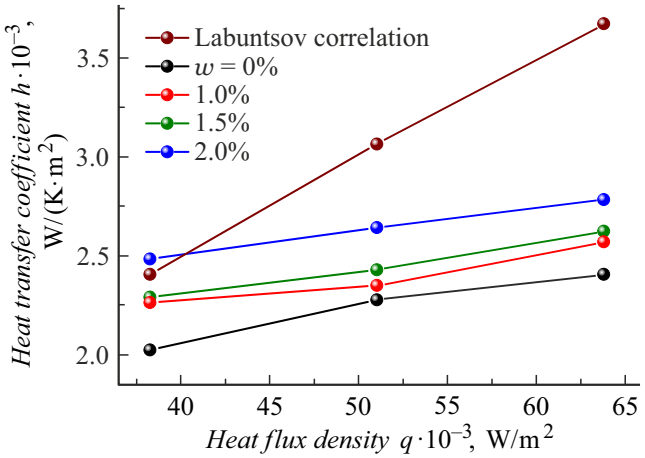

Figure 7. The impact of nanofluid on the heat transfer coefficient h at different mass concentrations of w nanoparticles (LTS1).

provided below [22]:

$$h = 0.075\left(1 + 10\left(\frac{\rho_v}{\rho_l - \rho_v}\right)^{0.67}\right)\left(\frac{k^2}{\eta_l/\rho_l\sigma T_s}\right)^{0.33} q_h^{0.67}, \quad (4)$$

which is also shown in Fig. 7 for pure water (the Rosenau correlation (1962) [23] gives similar results). The calculated and experimental values as can be seen from Fig. 7 are quite consistent at low heat flux (less than 40 kW/m^2); subsequently, the deviation gradually increases. This is due to the fact that the heat transfer mode in the LTS evaporator is not similar to the heat transfer when boiling in a large volume in the range of heat fluxes 45–65 kW/m^2. The HTC value also increases with increasing heat flux at all operating temperatures.

These results were obtained in 2012. Then LTS1 was left for storage for 6 years. Further studies of LTS1 were continued in May 2018. The results obtained are shown in Fig. 8.

The heat transfer coefficient did not changed within the measurement error as can be seen from the analysis of these data: the curve $w = 2\%$ (2018) approximately coincides with the curve $w = 2\%$ (2012). In this regard, the working fluid was removed from the thermosyphon and the iron oxide content (Fe_xO_y) was analyzed in samples (sampling of working fluid after work in LTS1). Atomic absorption spectrophotometer Shimadzu AA-7000 was used for the analysis. The concentration of iron oxide (Fe_xO_y) after 6 years of operation of LTS1 at 2% iron oxide content was 0.023% by weight (the relative standard deviation of the measurement results was 7.5%).

This means that the amount of iron oxide in the nanofluid filled in 2012 and extracted from LTS1 in 2018 differs by 90 times, i.e. iron oxide particles remained inside LTS1. In addition, LTS1 was again filled with pure distilled water after thorough pumping (up to a pressure of 10^{-2} mbar) of the coolant vapor (with its heating) and measurements of the heat transfer coefficient were repeated. These results are shown in Fig. 8 ($w = 0\%$ (2018)). It can be seen that these results correspond to the previously obtained data of nanofluid Fe_xO_y/(2% water). Thus, these experiments indicate the deposition of nanoparticles on the evaporative surface of the evaporator.

For this purpose, the evaporator was cut to visualize this surface and then analyze it using scanning electron microscopy (SEM). The results of this analysis are shown in Fig. 9. As can be seen, iron oxide particles settled on the evaporation surface (brownish color (in the online version) in Fig. 9, a), and then agglomerated (Fig. 9, *b*).

Thus, a micro-/nanorelief was formed on the evaporation surface, which apparently created conditions for increasing heat transfer from this surface and increasing the heat transfer coefficient [14].

The above studies of the LTS were aimed at its use for cooling LED modules and aimed to make the cooling system more flat, i.e. to reduce the distance between the heat source (evaporator) and the heat sink (condenser). A radiator was used as a heat sink in conditions of natural convection (in addition to an aluminum radiator, a radiator made of heat-dissipating plastic was tested) [14]. This circumstance limited the maximum heat transfer.

Subsequently, LTS2 was fabricated and tested with a high heat flux density in the transport zone (up to 6 kW/cm^2), which was ensured by small internal diameters of the steam and liquid channel 2 × 0.5 mm (Fig. 1) to transport the heat like the electricity is transported. In addition, small-section tubes improve the layout of the heat transfer system in real temperature control devices. A water-cooled condenser was used to improve the conditions of heat runoff. Distilled, deionized water and nanofluid — the same water with 2 mass% of copper oxide nanoparticles (Cu_xO_y) were used as a coolant. The filling volume was 38.5ml (55% of the total internal volume of LTS2 or 80% of the internal volume of the evaporator), which corresponded to the thickness of the liquid layer in the evaporator (in the absence of heat load) about 16 mm. Fig. 10 shows these coolants for LTS2

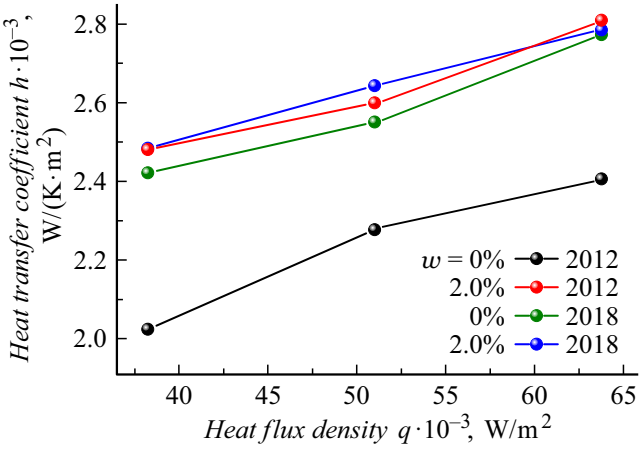

Figure 8. Degradation (aging) of nanofluid over time; $w = 2\%$ — mass concentration of nanoparticles (LTS1).

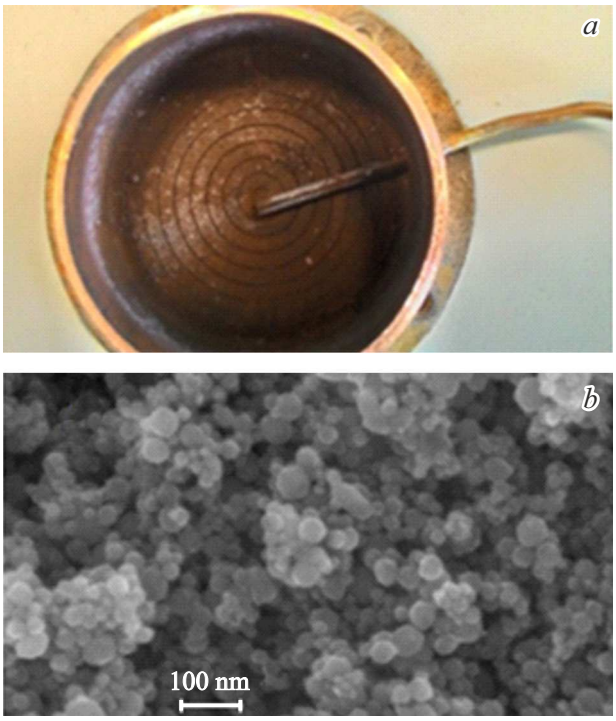

Figure 9. Possible explanation for the increase of heat transfer: *a* — vaporization surface in the evaporator LTS1; *b* — distribution of nanoparticles on the vaporization surface in the evaporator LTS1 (scanning electron microscopy (SEM), scale 100 nm).

after three months of their storage, where no changes in color are visually visible during this period, which indicates the absence of visible agglomeration and precipitation of nanoparticles.

Fig. 11 shows the characteristic temperatures of LTS2 over time depending on the heat load, respectively, other things being equal for distilled water (left) and nanofluid (right). The maximum heat flow is higher as can be seen from the presented data, and the corresponding temperatures of the heat source are lower for LTS2 with nanofluid.

Figures 12 and 13 show, respectively, the dependences of the heat transfer coefficient (HTC) h on the heat flux density q and thermal resistance R_t on the heat load Q.

The results presented in Fig. 12 indicate an increase of HTC when using nanofluid (in comparison with pure water) over the entire range of changes in heat flux density. At critical values of heat flux density (limitations are caused by hydraulic resistances in the transport zone in accordance with the calculation model below) this increase corresponds to an increase of HTC by more than 1.5 times. As for the thermal resistance (Fig. 13), the changes here are ambiguous. The thermal resistance of LTS2 is lower for water at low heat loads (up to 130 W), t, and for large heat loads (more than 150 W) Rt is 1.3 times higher for clean water.

Thus, the presented experimental data for the LTS indicate the advantages of using nanofluids as heat carriers.

2.2. On the calculation model of the maximum heat load LTS

The calculation of the hydrodynamic limit is based on the need for a driving force in the working state of the LTS, which causes the circulation of the working fluid from the evaporator to the condenser and back to close the evaporation-condensation cycle in it. This condition can be written as an inequality

$$\Delta P_g = \beta(\rho_l - \rho_v)gH \geq \Delta P_v + \Delta P_l, \qquad (5)$$

where ρ_l — density of the liquid phase; ρ_v — density of the vapor phase; H — hydrostatic pressure of the liquid column above the evaporator (the surface of the liquid in it), which actually returns the liquid to evaporator; ΔP_v and ΔP_l — hydraulic resistance (pressure drop) in the vapor and liquid phases, respectively. The typical value of the correction factor β for the nominal heat load is usually 0.75. Equality in the formula (5) means maximum heat transfer under these conditions.

Using the Hagen-Poiseuille equation for laminar steam flow and the Fanning equation for turbulent flow and taking into account the formulas for local and integral differential pressure coefficients, the final equation for maximum heat

Figure 10. The main heat carriers of LTS2: water (left) and water + 2% Cu_xO_y (right) after three months of storage.

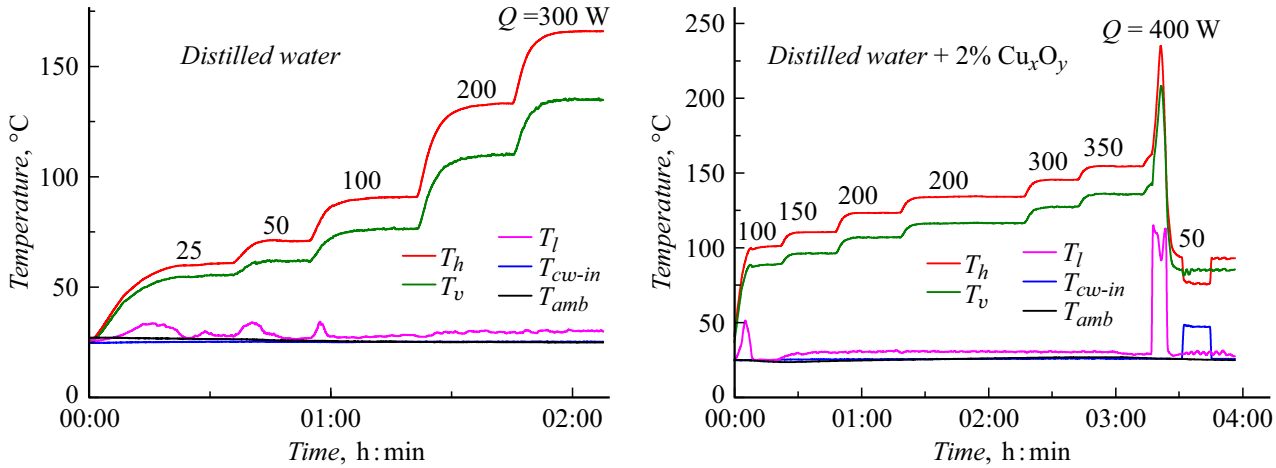

Figure 11. Basic temperatures of LTS2 with distilled water (left) and nanofluid (right) at various heat loads Q.

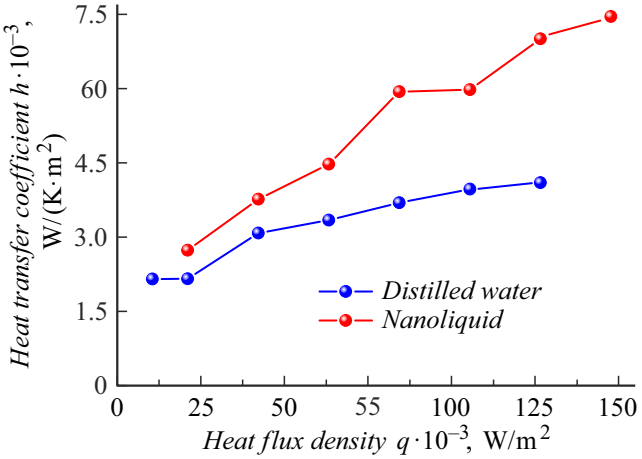

Figure 12. Dependence of the heat transfer coefficient h on the heat flux density q in the LTS2 evaporator with distilled water and nanofluid.

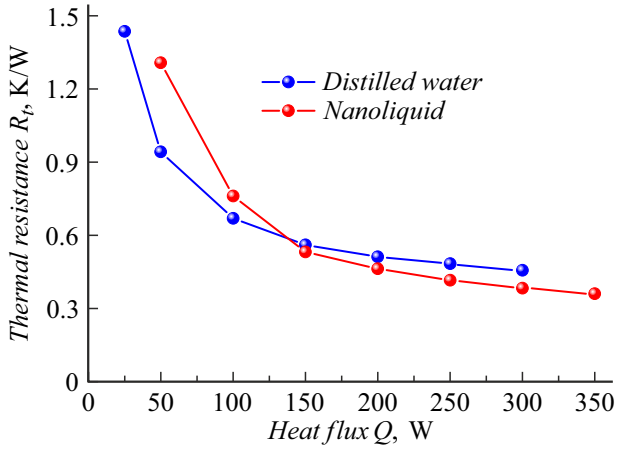

Figure 13. Dependence of the thermal resistance R_t on the heat flux Q In the LTS2 evaporator with distilled water and nanofluid.

flow Q will be as follows:

$$Q(H) = \begin{cases} \frac{\beta(\rho_l - \rho_v)gH}{(E+D)} & \text{for Re} \le 2100, \\ \frac{\beta(\rho_l - \rho_v)gH}{(C+D)} & \text{for Re} > 2100, \end{cases} \quad (6)$$

where

$$D = 128 \frac{\eta_l(T_l)}{\rho_l(T_l)} \frac{L_l}{\pi d_l^4} \frac{1}{H_{ev}(T_v)},$$

$$E = 128 \frac{\eta_v(T_v)}{\rho_v(T_v)} \frac{L_v}{\pi d_v^4} \frac{1}{H_{ev}(T_v)},$$

$$C = 0.6328 \text{Re}^{0.75} \frac{\eta_v(T_v)}{\rho_v(T_v)} \frac{L_v}{\pi d_v^4} \frac{1}{H_{ev}(T_v)},$$

$$\text{Re} = \frac{4Q(H)}{\pi d_v \eta_v(T_v) H_{ev}(T_v)}.$$

The above equation includes the physical properties of the liquid and vapor phases as a function of temperature (viscosity, density, specific heat of vaporization), as well as geometric and structural parameters of the LTS. Therefore, knowing the listed properties, it is possible to obtain a functional dependence of Q on H for laminar and turbulent flows, respectively.

Figure 14 shows the function $Q(H)$ for pure water at the temperature of steam and liquid according to experimental data (Figure 11) and the following contour parameters: equivalent length and diameter of the steam pipe $L_v = 1100$ mm, $d_v = 2$ mm, equivalent length and diameter of the liquid line $L_l = 900$ mm and $d_l = 2$ mm.

As can be seen from the figure, the selected model adequately describes the hydrodynamic limit in a loop thermosyphon ($Q = 350$ W at $H = 1.1$ m) even though the model does not take into account the boiling process, and does not take into account some details of the heat transfer mechanisms that occur at the boundaries of the liquid-vapor phase interface.

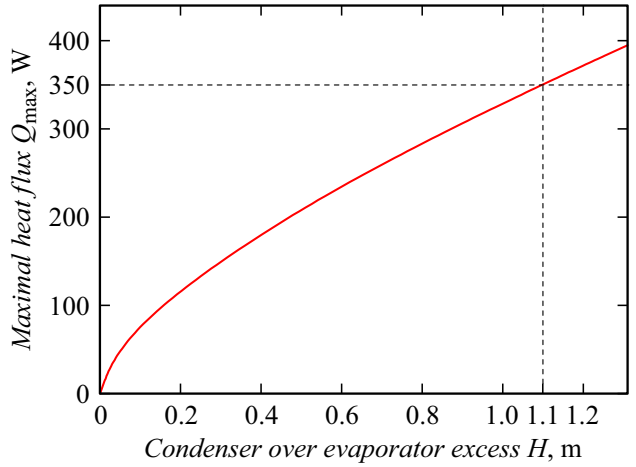

Figure 14. Dependence of the maximum heat flow Q_{max} on the distance H by which the height of the condenser exceeds the evaporator in LTS2.

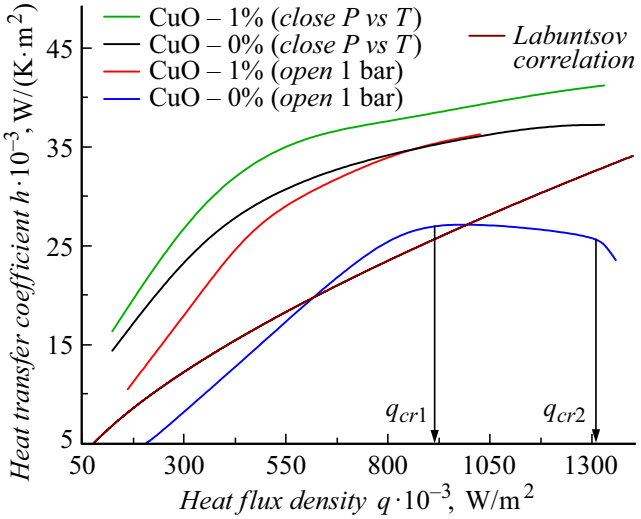

Figure 15. The impact of nanofluid on the heat transfer coefficient h at different mass concentrations of nanoparticles w .

2.3. Traditional thermosyphon with nanofluids

The experimental technique assumed obtaining data on the performance of the thermosyphon in the form of a relationship between the control temperatures and the heat load Q. Temperatures were measured at the points $A-G$ indicated in Fig. 3. Measurements were performed before and after the transition of the system to steady-state mode for each heat load Q. Figure 15 shows the main effect on the heat transfer coefficient (HTC) h for various mass concentrations ($w = 0$ and 1%) of nanoparticles (nanofluid copper oxide/water) and various pressures: for an open thermosyphon („open“) (pressure $P = 1$ bar) and for a closed („close“) thermosyphon ($P = P(T_v)$).

It was found that the impact of the refilling volume is insignificant. However, the minimum temperature corresponded to the refueling volume of 50 ml, which corresponded to the thickness of the liquid layer in the heat supply zone of the TTS evaporator (in the absence of heat load) about 20 mm, and further measurements were carried out with this refilling volume. At the same time, the thickness of the liquid layer (according to visual observations) varied from 20 to 8 mm, depending on the magnitude of the heat load.

The heat transfer coefficient (HTC) during vaporization was calculated using equation (3), where Q — heat load; S_h — the surface area of the supplied heat $3.14 \cdot 10^{-4}$ m^2; and T_{ev} and T_v — values of heater and steam temperature at points E and D (see fig. 3) respectively. The determination of the critical heat flow was fixed by decreasing HTC depending on $h = f(q)$.

The experimental results shown in Fig. 15 demonstrate the effect of mass concentrations on the increase of the evaporation temperature of the nanofluid ($w = 0$, 1.0 weight%), which indicates a significant increase of the heat transfer coefficient. The increase is 20−25% at a concentration of $w = 1.0$%. In addition, the value of CHF significantly increased (by 30%) compared to pure water. This indicates the efficiency of the use of nanofluids in traditional thermosyphons.

The curve calculated using the formula (4) HTC is also shown in Fig. 15. Due to the complexity of heat transfer in a thermosyphon, it is difficult to find predictive correlations to accurately calculate its HTC [24], therefore, a well-known empirical correlation proposed by Labuntsov [22] was used to calculate HTC when boiling pure water in a large volume.

As shown in Fig. 15, the calculated and experimental values agree well with the heat flow (less than CHF), but at values above the CHF level, significant differences are observed; subsequently, the deviation gradually increases. A detailed photo and video recording of the boiling process was carried out during the study of the thermosyphon. These results are shown in Fig. 16.

A conclusion about the difference between the boiling mechanism of pure water and nanofluid in a traditional thermosyphon can be made using the visualization of the boiling process. In the case of pure water, a geyser-like formation appears when boiling. In the case of nanofluid, a foamy state was observed. In our opinion, the explanation of this visual phenomenon is as follows. Liquids are somewhat self-purified from impurities during phase transformations and the impurities themselves are carried out into the thin-film part of the meniscus (which, due to the roughness of the vaporization surface, is always there). This is also evidenced by the results of our early experiments [25].

In the same way, apparently, the Rayleigh-Taylor instability is formed in dynamics, caused by temperature and gravitational convection in dispersed systems. We believe that a complex process of formation of this surface takes place on the surface of vaporization in dynamics, due to the fact that due to the heterogeneity of nanoparticles in size, large particles settle and agglomerate on the surface, and smaller ones form unstable convective cells near it, which

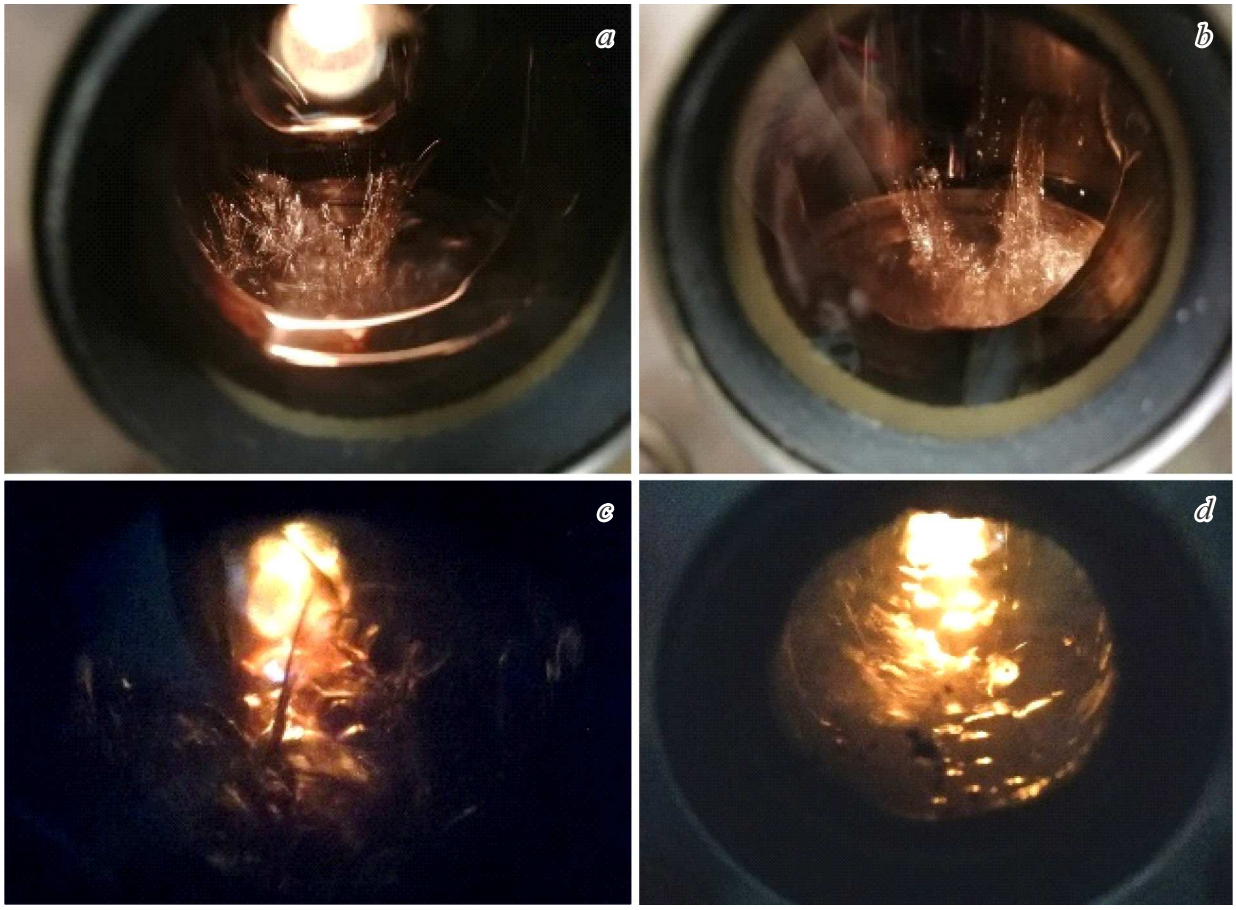

Figure 16. Visualization of the boiling process of pure water (a, b) and nanofluid (water/copper oxide) with a mass concentration of $w = 1\%$ (c, d) at low (a, c) and critical (b, d) heat flow in a closed system.

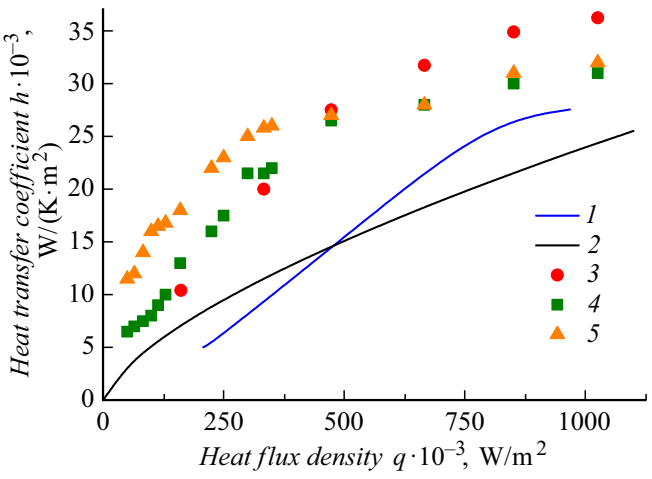

Figure 17. Comparison of heat transfer coefficients (HTC) and critical heat flux (CHF) (maximum values of HTC) for a traditional thermosyphon under conditions close to boiling in a large volume: *1* — pure water; *2* — Rosenau correlation [23]; *3* — nanofluid (water + 1% Cu_xO_y); *4* — three layers mesh (thickness 0.5 mm) with equivalent pore diameter 40 μm; *5* — porous titanium (thickness 1 mm) with equivalent pore diameter 8 μm.

leads to an intensification of heat exchange. We see the result of this complex process, presented in Fig. 9 in static (in the absence of intensive vaporization).

It is of interest to compare the heat transfer coefficient when boiling in a large volume for pure water on a technically smooth and porous surface, as well as when boiling nanofluid. These experiments were carried out on an installation (Fig. 3) with a cell (Fig. 4) sequentially, first for clean water, then for clean water with various porous surfaces with controlled preload to the heating surface: 3 layers of 0.5 mm thick mesh with an equivalent pore diameter of 40 μm porous titanium (thickness 1 mm) with equivalent pore diameter 8 μm and finally — with nanofluid. The amount of coolant filling was the same and was 50 ml. These data are shown in Fig. 17.

As can be seen from the figure, the HTC value of nanofluid is higher than that of pure water with a heat flux density of up to 500 kW/m^2, but lower than that of porous materials. However, the HTC value of the nanofluid becomes the highest with an increase of the heat flux density. At the same time, the value of CHF also increases: in comparison with pure water — by 30%.

Conclusion

The study of the heat transfer characteristics of loop and traditional thermosyphons using nanofluid Fe_xO_y/water and Cu_xO_y/water as heat carriers was studied in this paper.

The main results of the performed studies.

1. New thermal control devices, in particular, LTS with a nanofluid coolant, were proposed, tested and proved their efficiency for LED cooling.

2. A technique was developed for obtaining nanofluids Fe_xO_y/water and Cu_xO_y/water using nanopowders obtained by laser spraying of the target.

3. The impact of nanoparticles on the performance of the LTS was experimentally studied. The results obtained indicate that nanofluids are promising as a coolant in two-phase systems, effectively increasing the heat transfer coefficient to 25−50%. The mass concentration of nanoparticles increases the heat transfer coefficient and, consequently, reduces the thermal resistance of the LTS compared to pure water.

4. The impact of nanoparticles on the performance of a traditional thermosyphon was experimentally studied. It is shown that nanofluids are promising as a working fluid in two-phase systems, effectively increasing the heat transfer coefficient to 20−25%. In addition, the CHF value significantly increased (by 30%) compared to pure water, which indicates the effectiveness of using nanofluids in traditional thermosyphons.

5. Visualization of the boiling process revealed the difference between the boiling mechanism of pure water and nanofluid in a traditional thermosyphon. In particular, the boiling of pure water looks geyser-like, while the boiling nanofluid is a foamy substance. Apparently, the Rayleigh-Taylor instability is formed in dynamics, caused by temperature and gravitational convection in dispersed systems. A complex process of formation of this surface occurs in dynamics on the surface of vaporization, due to the fact that due to the heterogeneity of nanoparticles in size, large particles settle and agglomerate on the surface, and smaller ones form unstable convective cells near it, which leads to an intensification of heat exchange.

6. A study of the stability of nanofluid showed that nanoparticles tend to agglomerate and settle on the evaporation surface over time, forming a pulsating nanorelief on the surface in dynamics, which improves heat/mass transfer during germinal boiling compared to a technically smooth surface.

Funding

We express our gratitude for the support from the Ministry of Education and Science of the Russian Federation within the framework of the State Assignment for Higher Education Institutions (research project № FEUZ-2023-0022).

Conflict of interest

The authors declare that they have no conflict of interest.

Notations

T — temperature, [K]; w — weight concentration, [%]; g — gravity acceleration, [m/s^2]; P — pressure, [Pa]; L — length, [m]; Q — heat flux, [W]; S — area, cross section, [m^2]; H — height, excess, [m]; Re — Reynolds number; q — heat flux density, [W/m^2]; d — diameter, [m]; k — thermal conductivity coefficient , [W/(K·m)]; h — heat transfer coefficient, [W/(K·m^2)]; H_{ev} — specific heat of vaporization, [J/kg]; V_l — coolant filling volume, [ml]; T_s — saturation temperature; $\dot{m}$ — mass flow rate, [kg/s].

Greek symbols

$\beta \leq 1$ — correlating factor of hydrostatic potential utilization; δ — thickness, [m];η — dynamic viscosity, [Pa·s]; ρ — density, [kg/m^3]; σ — surface tension coefficient, [N/m].

Indices

LTS — Loop thermosyphon, TTS — traditional thermosyphon, amb — environment, cw — cooling water, ev — evaporator, g — hydrostatic, in — input, out — output, l — liquid, v — steam, h — heater.

References

[1] S.U. Choi, J.A. Eastman. *Enhancing Thermal Conductivity of Fluids With Nanoparticles* (No. ANL/MSD/CP-84938; CONF-951135-29). Argonne National Lab.(ANL), Argonne, IL (USA, 1995)

[2] S.K. Das, N. Putra, P. Thiesen, W. Roetzel. J. Heat Transfer, **125** (4), 567 (2003).

[3] J.A. Eastman, S.U.S. Choi, S. Li, W. Yu, L.J. Thompson. Appl. Phys. Lett., **78** (6), 718 (2001).

[4] D. Wen, Y. Ding. Intern. J. Heat and Mass Transfer, **47** (24), 5181 (2004).

[5] Y. Xuan, Q. Li. Intern. J. Heat and Fuid Flow, **21** (1), 58 (2000).

[6] A. Asadi, F. Pourfattah, I.M. Szilágyi, M. Afrand, G. Żyła, H.S. Ahn, O. Mahian. Ultrasonics Sonochemistry, **58**, 104701 (2019).

[7] S.K. Das, N. Putra, W. Roetzel. International J. Heat and Mass Transfer, **46** (5), 851 (2003).

[8] S. Khandekar, Y.M. Joshi, B. Mehta. Intern. J. Thermal Sci., **47** (6), 659 (2008).

[9] Y.H. Lin, S.W. Kang, H.L. Chen. Appl. Thermal Eng., **28** (11−12), 1312 (2008).

[10] S.W. Kang, W.C. Wei, S.H. Tsai, C.C. Huang. Appl. Thermal Eng., **29** (5−6), 973 (2009).

[11] K.H. Do, S.P. Jang. Intern. J. Heat and Mass Transfer, **53** (9−10), 2183 (2010).

[12] Z.H. Liu, X.F. Yang, G.L. Guo. Intern. J. Heat and Mass Transfer, **53** (9−10), 1914 (2010).

[13] G. Huminic, A. Huminic, I. Morjan, F. Dumitrache. Intern. J. Heat and Mass Transfer, **54** (1−3), 656 (2011).

[14] V. Kiseev, O. Sazhin. Intern. J. Heat and Mass Transfer, **132**, 557 (2019).

[15] A. Kamyar, K.S. Ong, R. Saidur. Intern. J. Heat and Mass Transfer, **65**, 610 (2013).
[16] H. Shabgard, B. Xiao. Intern. J. Heat and Mass Transfer, **70**, 91 (2014).
[17] K. Cacua, R. Buitrago-Sierra, E. Pabon, A. Gallego, C. Zapata, B. Herrera. Intern. J. Thermal Sci., **153**, 106347 (2020).
[18] L.A. Shuoman, M. Abdelaziz, S. Abdel-Samad. Heat and Mass Transfer, **57**, 1275 (2021).
[19] D.Y. Aydín, E. Çiftçi, M. Gürü, A. Sözen. Energy Sources, Part A: Recovery, Utilization and Environmental Effects, **43** (12), 1524 (2020).
[20] V.B.J.A.G. Bhuibhar, P.P. Pande. Intern. J. Eng. Sci. Res. Technol., **7** (3), 51 (2018).
[21] H. Ghorabaee, M.R.S. Emami, N. Karimi, F. Moosakazemi. Powder Technol., **394**, 250 (2021).
[22] D.A. Labuntsov. Thermal Engrg., **19**, 21 (1972).
[23] W.M. Rohsenow. J. Fluids Eng., **74** (6), 969 (1952).
[24] A. Sathyabhama, R.N. Hegde. Thermal Sci., **14** (2), 353 (2010).
[25] A.G. Belonogov, V.M. Kiseev. AICHE Symposium Ser., **91** (306), 333 (1995).

Translated by Ego Translating